# Transmembrane potential modeling: Comparison between methods of constant electric field and ion imbalance.

Josef Melcr,[†] Daniel Bonhenry,[†] Štěpán Timr,[†] and Pavel Jungwirth[*,†,‡]

*Institute of Organic Chemistry and Biochemistry, Czech Academy of Sciences, Flemingovo nám. 2, 16610 Prague 6, Czech Republic, and Department of Physics, Tampere University of Technology, P.O. Box 692, FI-33101 Tampere, Finland*

E-mail: jungwirth@uochb.cas.cz

**Abstract**

Two approaches for modeling of the transmembrane potential, as present in all eukaryotic cells, are examined in detail and compared with each other. One approach uses an externally applied electric field, whereas the other maintains an imbalance of ions on the two sides of a membrane. We demonstrate that both methods provide converged results concerning structural parameters of the membrane which are practically indistinguishable from each other, at least for monovalent ions. Effects of the electric field on the detailed molecular structure of the phospholipid bilayer are also presented and discussed. In addition, we achieve a considerable speed-up of the underlying molecular dynamics simulations by implementing the virtual interaction sites method for the Slipids force field.

[*]To whom correspondence should be addressed
[†]Institute of Organic Chemistry and Biochemistry
[‡]Tampere University of Technology

# 1 Introduction

All eukaryotic cells maintain a non-zero transmembrane potential across their plasma membranes. The voltage difference from the exterior of the cell in a resting state to the interior is usually in the range from -10 to -100 mV.[1,2] Its magnitude is determined by the permeability of the membrane to specific ionic species via ion channels, by the intra- and extra-cellular ionic distributions, as well as by active ion transport across the membrane.[2] In neurons, changes in the membrane potential enable these cells to conduct electrical signals along their axons. In the resting state of the neuron, the transmembrane voltage has a value around -70 mV.[2] During neural activity, however, the transmembrane potential undergoes a dramatic change. This process happens in the range of milliseconds, and it is mainly driven by the action of sodium and potassium channels. The openings and closings of these channels induce non-zero fluxes of ions across the membrane. This leads to a sudden polarity inversion of the transmembrane voltage, which then propagates along the neural axon. This avalanche process of membrane depolarization is called an action potential.[2]

In experiments, the transmembrane potential can be monitored using microelectrodes[3,4] or voltage-sensitive fluorescent probes.[5–13] The information about the transmembrane potential obtained from the experiment is of a limited microscopic resolution, showing features like current-voltage characteristics. In contrast, computer simulations, such as molecular dynamics, provide an atomistic picture of the system. To date, there exist two methods for modeling of the transmembrane potential in molecular simulation – the constant electric field method[14–18] and the ion imbalance method.[19,20] Both of these methods have been successfully used to study the electroporation phenomenon or to induce a transmembrane voltage when a voltage-sensitive protein was embedded within a lipid bilayer.[17,21–24]

The constant electric field method originates from the Poisson-Boltzmann theory.[16] Within this theory, the transmembrane potential is represented by an external electric field applied in the direction of the membrane normal.[16] Such a field then acts on every atom in the system proportionally to their partial charges and the field strength. This additional force

represents the influence of a voltage source far in the bulk, which is an effective simplified model of the biological apparatus, i.e., ion pumps and channels, responsible for the existence of the transmembrane voltage in cellular membranes. In periodic systems, commonly used in molecular simulation, the electric field is homogeneous.[16] The potential difference $V$ across the membrane is then the field intensity $E_z$ multiplied by the simulation box length $L$ parallel to the membrane normal, $V = E_z \cdot L$. It is worth noticing that for modeling of currents through membrane pores or channels this method is prone to finite-size artifacts arising from system fluctuations providing enhanced fluxes.[16,17,20] This also raises a concern for the modeling of membrane electroporation with short nanosecond electric pulses as the small system size may lead to an artificial redistribution of ions not observed in the experiments.[25] Finally, it is still an open question how this method performs when the electrolyte also contains divalent ions like $Ca^{2+}$, which are known to be described poorly within the Poisson-Boltzmann theory.[26]

In the ion imbalance method the voltage drop is introduced via a net charge difference between separated ionic solution reservoirs.[19,20] The voltage drop across the membrane then depends on the amount of excess charge (ions in this case) forming the imbalance and the membrane capacitance. This setup is meant to mimic the steady state condition of biological membranes with a meta-stable ionic distribution, without explicitly representing the underlying biological apparatus. In simulations with periodic boundary conditions, the excess ions are kept in imbalance by introducing a second membrane[19] or a solution/vapor interface.[20] Although the setup with a solution/vapor interface has the advantage of simulating only a single bilayer, it also requires a change from a tensionless to a constant volume ensemble and may be prone to artifacts due to the presence of the free water surface. The double bilayer setup with two separate electrolyte reservoirs avoids this problem at the cost of a significantly increased number of atoms in the simulation. Within the frame of the ion imbalance method, the field and voltage tend to substantially fluctuate around their mean values.[16] Also, the voltage drop is not a priori known and it is not trivial to fine tune it to a precise

value.

Both of these modeling approaches have been applied for simulating membrane potentials.[17,22,23,27] In several studies, the methods are also compared as representatives of different classes of electroporation experiments.[20,24,25,28] However, a detailed comparison of the methods in terms of equivalence of the generated electric field effects is missing. In this article, we aim at having a more thorough look at the two methods, comparing them by focusing on several key properties such as profiles of the transmembrane potential and the electric field intensity, charge and ionic densities, membrane capacitance, and water and lipid ordering.

# 2 Methods

## 2.1 Simulation details

The simulated systems consisted of two lipid bilayers separated by aqueous salt solutions. The lipid bilayers were composed of 64 1-Palmitoyl-2-oleoylphosphatidylcholine (POPC) molecules per leaflet spanning the $xy$-plane of the periodic simulation box. A modified Slipids force field[29,30] was used for their description (see also the following section 2.2). They were hydrated with 10240 TIP3P water molecules.[31] 112 water molecules were eventually replaced by ions to form a KCl or NaCl salt solution. Due to interactions of ions with the bilayers, their bulk concentration is lower than the nominal one, approaching thus physiological values. The parameters for the ions were taken from the references.[32,33] Classical molecular dynamics simulations were performed using the GROMACS[34] simulation package (version 4.6.7). The simulation input parameters are based on the settings used in the original Slipids publication.[30] The simulation settings used in this work are summarized in Table 1; more details are given in the Supporting Information (SI).

Molecular dynamics simulations of membranes require relatively long timescales for generating reliable statistical ensembles.[27,41,42] Based on convergence patterns of various distributions, such as the charge density profiles, a sufficient simulation time was estimated to

Table 1: Simulation parameters

| simulation property | parameter |
|---|---|
| time-step | 6 fs (using virtual interaction sites) |
| long-range electrostatics | PME[35] |
| external electric field intensity | 0.0 or 0.066 V/nm |
| cut-off scheme | Verlet[36] |
| Coulomb and VdW cut-off | 1.0 nm |
| simulation time | 300 ns |
| temperature | 310 K |
| thermostat | v-rescale[37] |
| barostat | Parrinello-Rahman, semi-isotropic[38] |
| constraints | LINCS, all bonds and virtual sites[39] |
| constraints for water | SETTLE[40] |

be around 200 ns. Thus, we performed 300 ns long simulations in the production run. All production runs were preceded with a pre-equilibration of a length on the order of 10 ns.

## 2.2 Virtual interaction sites

The fastest degrees of freedom are most often associated with the motions of hydrogen atoms in biomolecular simulations. Virtual interaction sites (VIS) is a method that removes these degrees of freedom and reconstructs such atoms in their ensemble-average positions using the coordinates of their neighboring atoms.[43] The speed, efficiency, and success of the VIS method for proteins has motivated us to develop also a lipid model which employs this approach.[44–46] For its good performance[47] we based this lipid model on the Slipids force field.[29,30] To our knowledge, the first attempt to apply the VIS method to lipids used the CHARMM36 force field.[46] In that study, however, the VIS method rendered the membrane to be more disordered than without applying it. This might have come from the fact that the average angle of the H−C−H groups in the fatty acid chains was overestimated by approximately five degrees.[46]

We observed a similar behavior when we applied the VIS method to the Slipids force field[29,30] in the same way as done previously for the CHARMM36 force field.[46] In contrast with the previous work, we then performed a proper averaging of the H−C−H angles of the

$CH_2$ groups in the fatty acid chains. We optimized this VIS model of Slipids to such a degree that it provided almost identical results to the original Slipids with a significant speed-up of the calculations by roughly a factor of three. More details can be found in the SI. We denote this new fast-running version of Slipids[29,30] as Slipids–VIS. The simulation files, the modified Slipids force field and the POPC topology with virtual sites designed for the use with the GROMACS package[34] used in this work are accessible at `http://dx.doi.org/10.5281/zenodo.47649`.

### 2.3 Poisson equation for transmembrane potential

In this work, we discuss two models of the transmembrane potential applicable in combination with molecular dynamics simulations. The transmembrane potential profile, $\Psi(z)$, $z = 0\,\text{to}\,L$, is thus a property of a central interest. Such a profile is obtained from the charge density profile using the Poisson equation in one dimension:[26]

$$\Psi(z) = -\frac{1}{\epsilon_0}\int_0^z dz' \int_0^{z'} \rho(z'')dz'' \tag{1}$$

Evaluation of the integrals in Equation 1 is complicated by fluctuations of the simulation box. It is thus important to properly center the bilayers along the trajectories such that the resulting profiles are not inconsistently smeared along the fluctuating $z$-axis.[27] It is, however, even more important to use a proper value of the box length in the $z$-dimension, $L$, in Equation 1. This is especially true for a comparison of potential profiles and voltage drops, which scale quadratically with this length. For the comparison of potentials in this work we hence employ the average value of $L = 14.8\,\text{nm}$ as obtained from all simulations and use it consistently in Equation 1.

## 3 Results and Discussion

Four types of simulations were performed in this study:

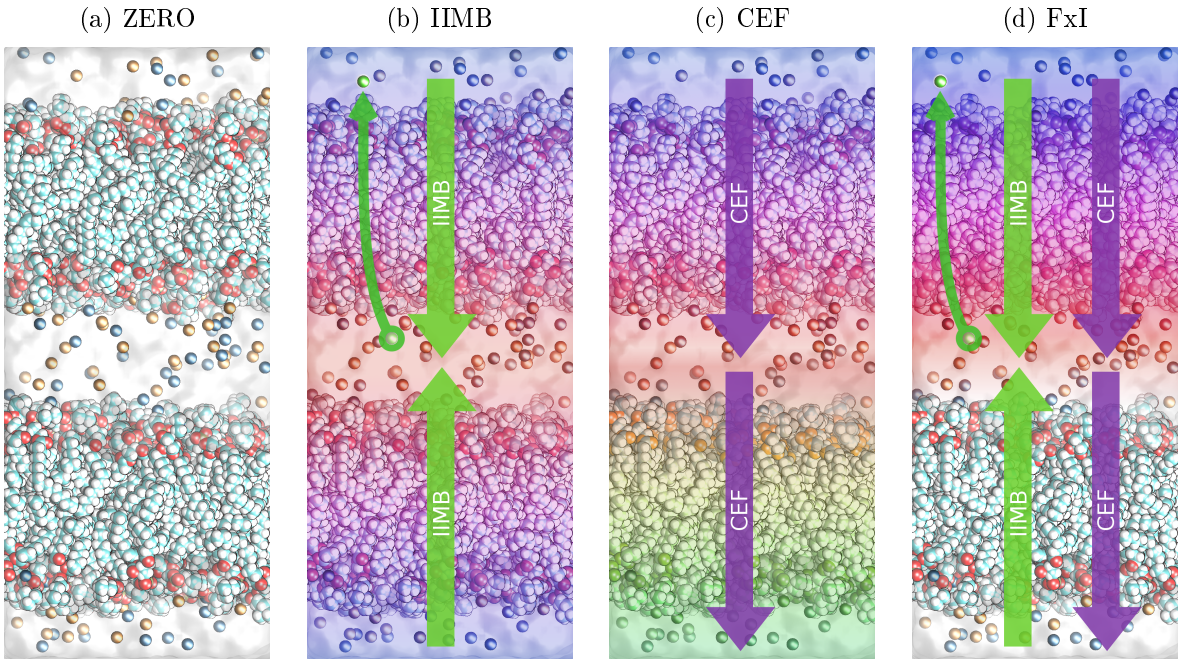


Figure 1: Schematic description of the four types of simulations performed in this work. The blue, red and green hue patterns qualitatively depict the voltage drops across the membranes. The violet arrows depict the electric field created by the CEF method, while the green arrows represent the field due to the IIMB scheme.

- Reference simulations with no applied voltage, denoted as ZERO (Fig. 1a),
- Simulations employing the ion imbalance method (IIMB) with a single ion transferred from one electrolyte to the other (Fig. 1b),
- Simulations using the constant electric field method (CEF) with such a field intensity that the voltage drop matches that from the ion imbalance simulations (Fig. 1c),
- Simulations with both methods applied simultaneously such that the generated electric fields cancel each other in one of the two bilayers, denoted as FxI (Fig. 1d).

The last type of simulations, FxI, uses the mirror-symmetric (with respect to the center of the box) IIMB method in combination with the CEF method, which has a translational symmetry. Hence, the potential drop is canceled across one membrane, while it is doubled across the other membrane (not used for analysis here). It is worth noticing that the former

membrane at zero voltage shares its lateral dimensions with the other membrane inducing a small difference from the conditions of ZERO simulations, where both membranes are at zero voltage.

Although the formalism for the CEF method was derived and applied only to systems with a single membrane,[16] we performed the CEF simulations with exactly the same configuration as in the IIMB simulations, i.e., with two membranes. This is a valid extension of the CEF method for periodic systems, in which the total voltage drop across the whole system splits in the exact same fractions for each of the two simulated bilayers. An example of an electrostatic potential profile of the whole system with two membranes is given in the SI.

## 3.1 Charge density, electric field intensity, and transmembrane potential

We performed the four types of simulations (ZERO, IIMB, CEF, and FxI) using either KCl or NaCl salt solutions as representatives of intracellular or extracellular electrolytes. For both electrolytes, the pairs of simulations IIMB and CEF, as well as ZERO and FxI provide each matching electrostatic potential profiles within a statistical error of about 7 mV, estimated using a block averaging scheme (Figs. 2 and 3). Moreover, the corresponding profiles in the two electrolytes are very similar to each other. In addition, the electrostatic potential profiles confirm that the potential drops occur practically exclusively across the low-dielectric interior of the membrane. Upon exerting a voltage drop across the membrane, the electrostatic potential profile responds with a perfectly linear inclination in its central part (Figs. 2, 3, and 4).

The first derivative of the potential, i.e., the electric field intensity, follows the fine match of the potential profiles for the different methods and electrolytes (Figs. 2 and 3). The changes of the electrostatic properties along the membrane normal are exemplified in the plots of the induced electric intensity; it is indeed only the central part of the profile that gives rise to a non-zero induced electric field, which is approximately constant in the cen-

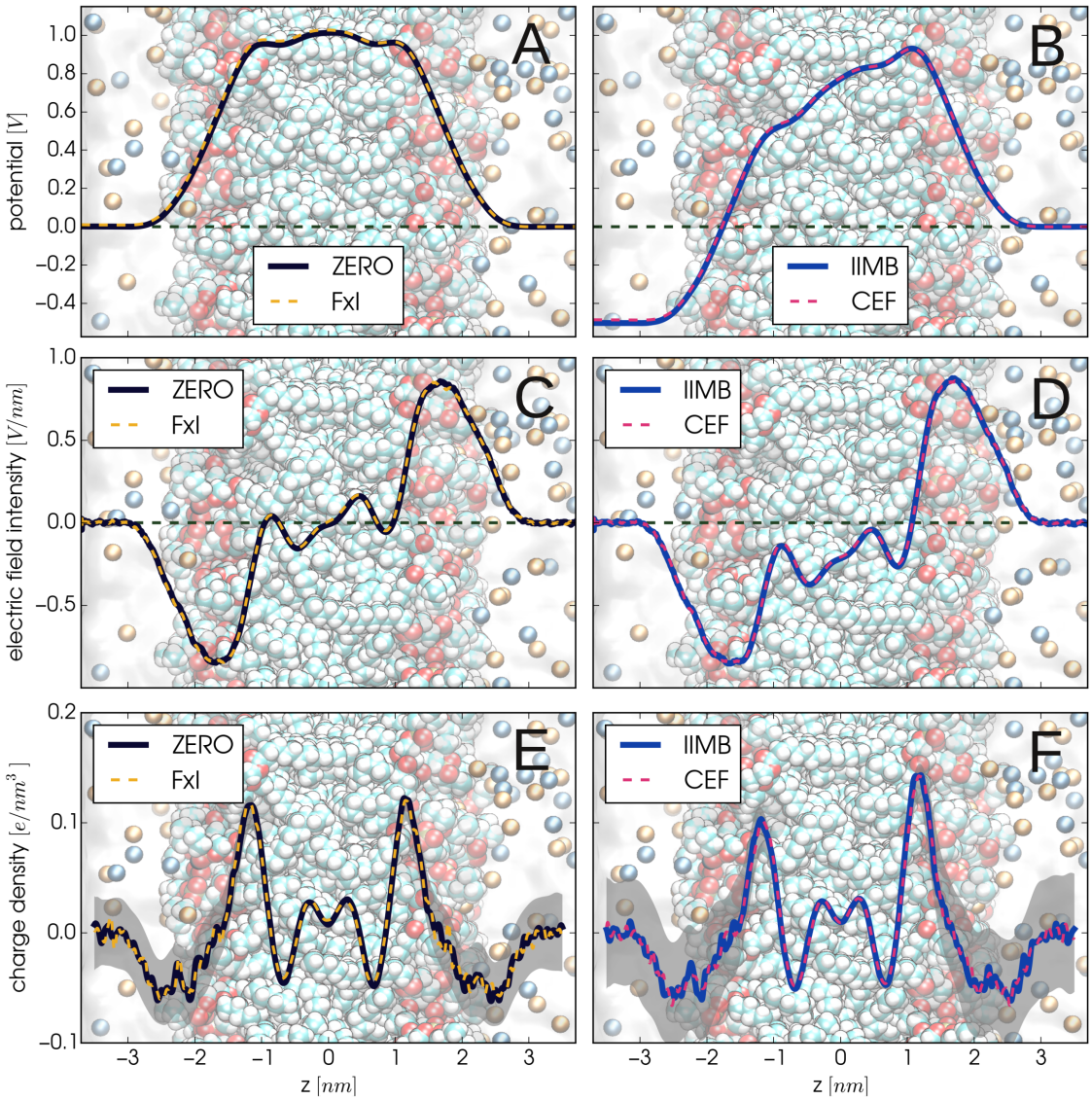


Figure 2: The transmembrane potential (A,B), the electric field intensity (C,D), and the charge density (E,F) profiles for the simulations with KCl. The gray area shows the standard error. The voltage drop across the membrane is 499 mV for IIMB and 486 mV for CEF with the error of about 7 mV.

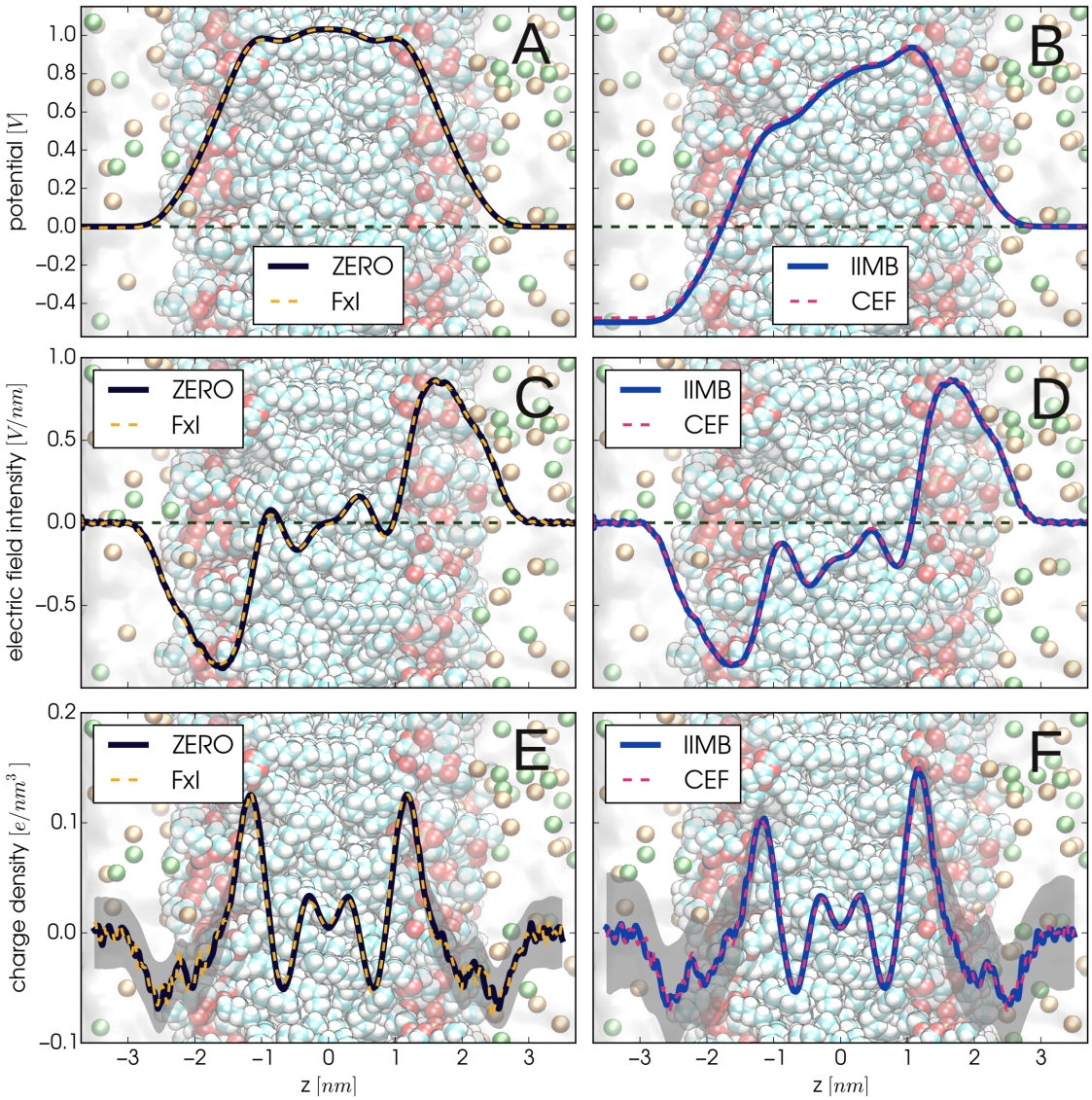


Figure 3: The transmembrane potential (A,B), the electric field intensity (C,D), and the charge density (E,F) profiles for the simulations with NaCl. The gray area shows the standard error. The voltage drop across the membrane is 499 mV for IIMB and 486 mV for CEF with the error of about 7 mV.

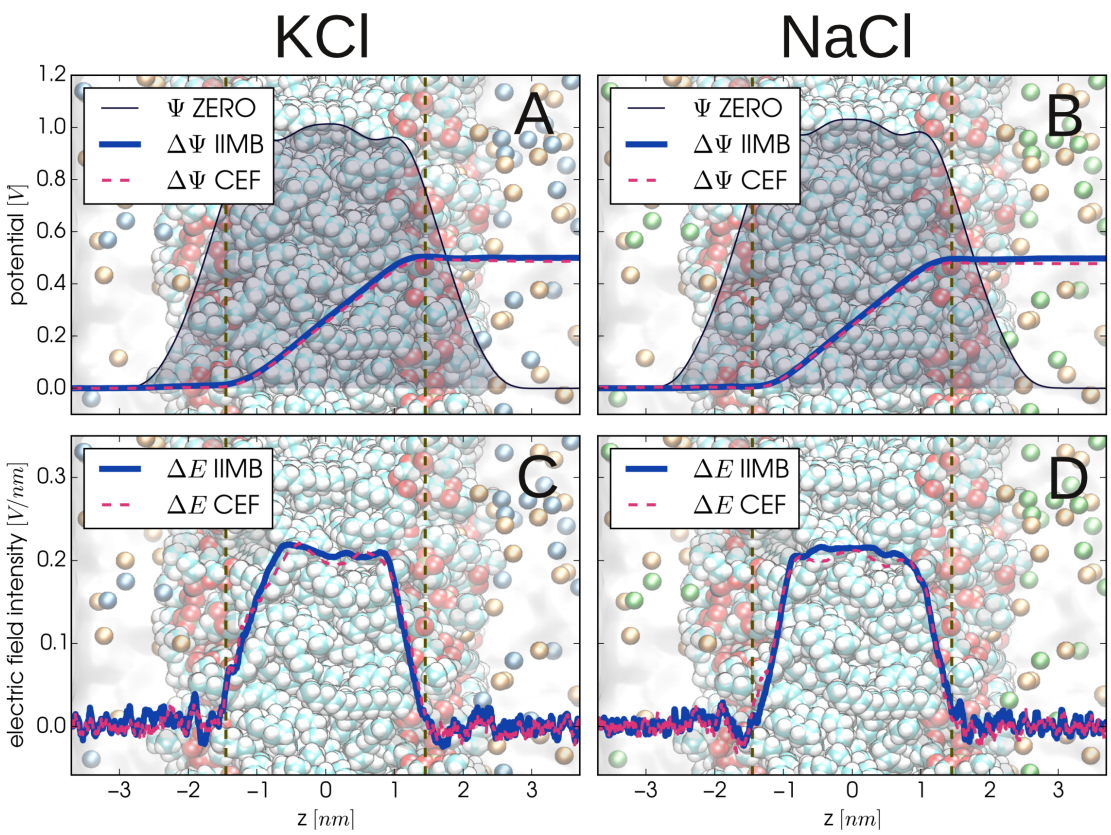


Figure 4: The difference of IIMB and CEF simulations from ZERO in the transmembrane potential (A,B) and the electric field intensity (C,D). The shadowed area shows the transmembrane potential profile of the ZERO simulations. The induced electric field is approximately constant and exists exclusively within the low-dielectric region of the membrane fatty interior. The vertical dashed lines denote the mean positions of the carbonyl groups.

ter of the bilayer (Fig. 4). This finding supports the approximative assumptions in the Goldman-Hodgkin-Katz equations for the electrostatic potential differences across membranes.[2,48] These equations assume the membrane to exist in a "Goldman regime" that approximates the real electrostatic potential within the membrane with a linear function resulting in a constant electric field.[2,48]

The charge density is the basic quantity upon which both the electrostatic potential and the field intensity are built. Because of a high residual noise, the charge density profiles do not show such a perfect match for the different methods and electrolytes as in the case of the potential and field intensity profiles. Also, there is a small systematic difference in ionic

(a) KCl (b) NaCl

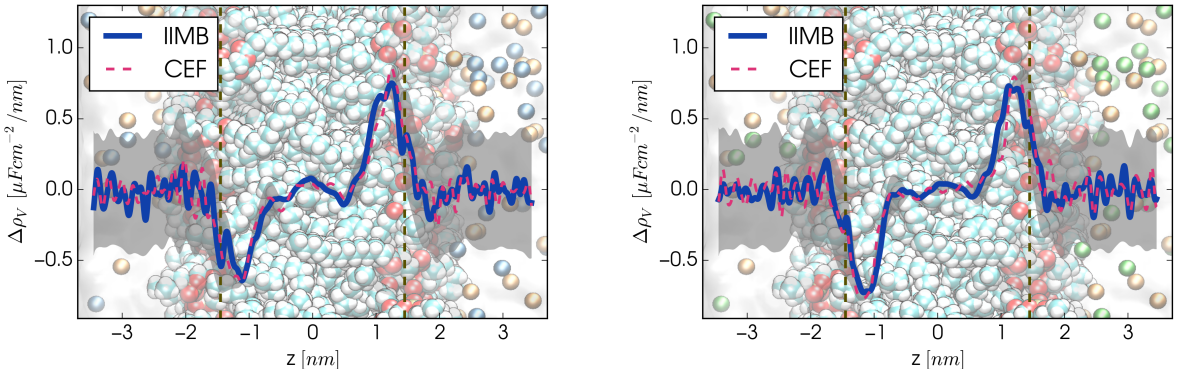


Figure 5: Profiles of the voltage-normalized differential charge density, $\Delta\rho_V$, using ZERO as a reference. The main charge redistribution takes place in the carbonyl region of the POPC membrane. The dashed vertical lines denote the mean position of carbonyl groups. The gray area shows the standard error.

concentrations up to 6 mM between the constant electric field and ion imbalance methods due to the effective transfer of a single ion in the latter. Still, they agree very well for both pairs of methods within the error bars. The voltage-induced changes are mainly reflected in the amplitudes of the highest peaks (Figs. 2 and 3).

## 3.2 Ionic and voltage-normalized differential charge densities, and membrane capacitance

The capacitance of a system is a quantity that reflects the response of a charge to the modulation of the electrostatic potential. The observed charge profiles consistently show the redistribution of an amount of charge $Q$ linearly proportional to the voltage $V$ with the capacitance of the membrane $C$, $Q = CV$, independently of the membrane voltage-inducing method. For the sake of a detailed comparison of the two methods employed here, we use a voltage-normalized differential charge density, $\Delta\rho_V(z)$, which reflects the contributions of individual layers along the membrane normal to the total capacity $C$. The voltage-normalized differential charge density is easily obtained from the simulations using the below Equation 2

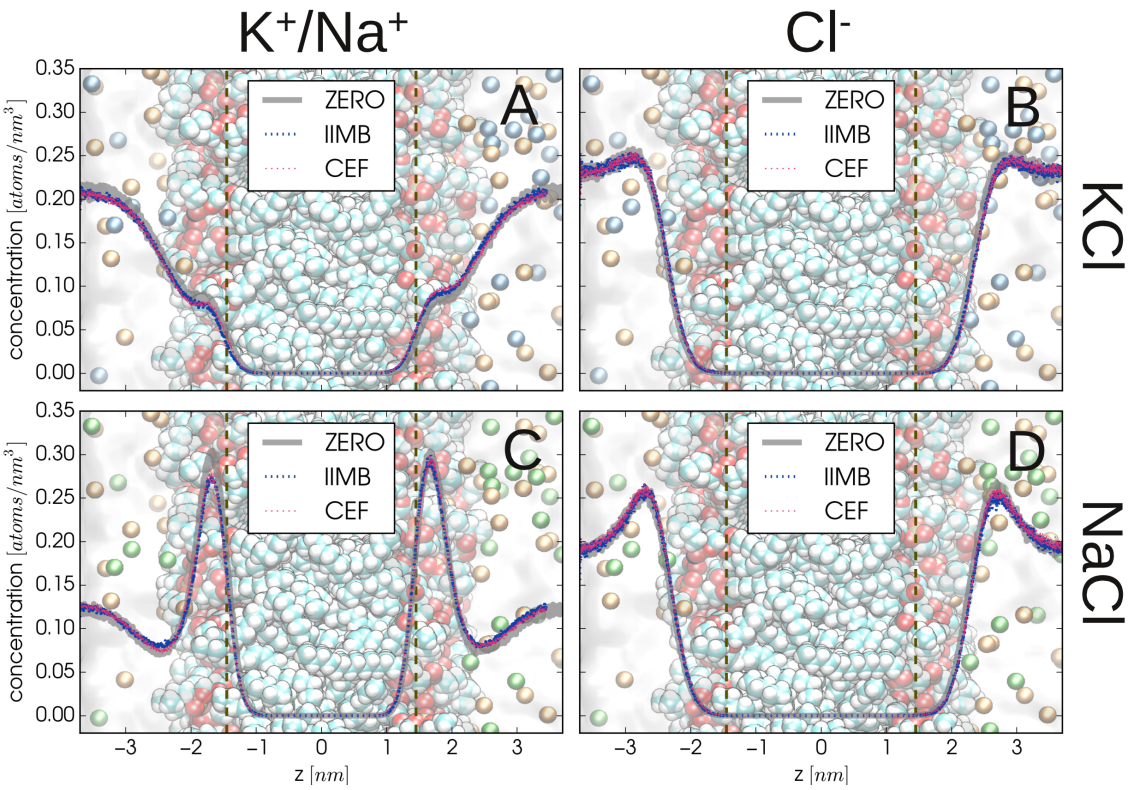


Figure 6: Ionic concentration profiles for $K^+$ and $Cl^-$ in KCl simulations (A,B), and $Na^+$ and $Cl^-$ in NaCl simulations (C,D). The cations accumulate at the side of the membrane with a positive potential (here at the right leaflet, see Figs. 2 and 3), whereas anions remain almost unaffected by the voltage. The dashed vertical lines show the mean position of carbonyl groups.

with $\Delta\rho(z)$ being the difference in the charge density between a simulation with an applied voltage and the ZERO simulation serving as a reference. In this relation it is assumed that $\Delta\rho(z)$ responds linearly to the voltage $V$ at each point $z$.

$$\Delta\rho_V(z) = \frac{\Delta\rho(z)}{V} \tag{2}$$

The $\Delta\rho_V(z)$ density profiles reveal the regions which are most affected by the charge redistribution (Fig. 5). Independently of the type of electrolyte, the highest peaks of this quantity appear just below the carbonyl region of the membrane. This is also reflected in the density profiles of the $K^+$, $Na^+$, and $Cl^-$ ions, which are the only free charge carriers (Fig. 6).

The layer with the largest changes in the charge density is at the interface of the low dielectric fatty interior of the membrane and its polar headgroup region. Namely, the largest change for cations is in the carbonyl and phosphate region, while for chloride ions it is shifted further toward the aqueous solution (roughly at the choline region, Figs. 6 and 5). This behavior is present both for NaCl and KCl electrolytes despite the fact that the $K^+$ cations do not penetrate into the membrane as much as the $Na^+$ cations (Fig. 6). The total capacitance of the simulated POPC membrane for the IIMB as well as the CEF methods and for both electrolytes is $C = (0.38 \pm 0.06)\,\mu\mathrm{Fcm}^{-2}$, which is somewhat lower than the experimental value of $(0.59 \pm 0.15)\,\mu\mathrm{Fcm}^{-2}$ [49] but still within the error bars. The membrane capacitance, $C$, can be obtained from the simulations using the basic the equation for capacitors, $Q = CV$, or by using the below Equation 3, which employs the voltage-normalized differential charge density, $\Delta\rho_V(z)$.

$$C = \frac{1}{2}\left|\int_{-L/2}^{L/2} \Delta\rho_V(z)\,\mathrm{sign}(z)\,dz\right| \tag{3}$$

The form of Equation 3 assumes that the membrane center is located at $z = 0$; $L$ is the simulation box-length, and $\mathrm{sign}(z)$ is a sign function yielding $-1$ for negative arguments and 1 otherwise. Because of the similarity between the formulas for the capacitance, $C$, and the differential charge density, $\Delta\rho_V(z)$, we express the latter in units commonly used for capacitance, i.e., $\mu\mathrm{Fcm}^{-2}$.

## 3.3 Water and lipid ordering

The ordering of water and lipids were chosen as quantities demonstrating the effects of the transmembrane voltage on molecular dipoles. Water dipoles are randomly oriented in the bulk where their average projection to the $z$-axis is zero. The hydrogen-bond network is more ordered close to the membrane interface where the water dipoles orient preferentially from the positive moieties (choline groups) to the negative moieties (phosphate groups) of the DOPC lipids.[50] With a zero transmembrane voltage the water dipoles orient in opposite

(a) KCl (b) NaCl

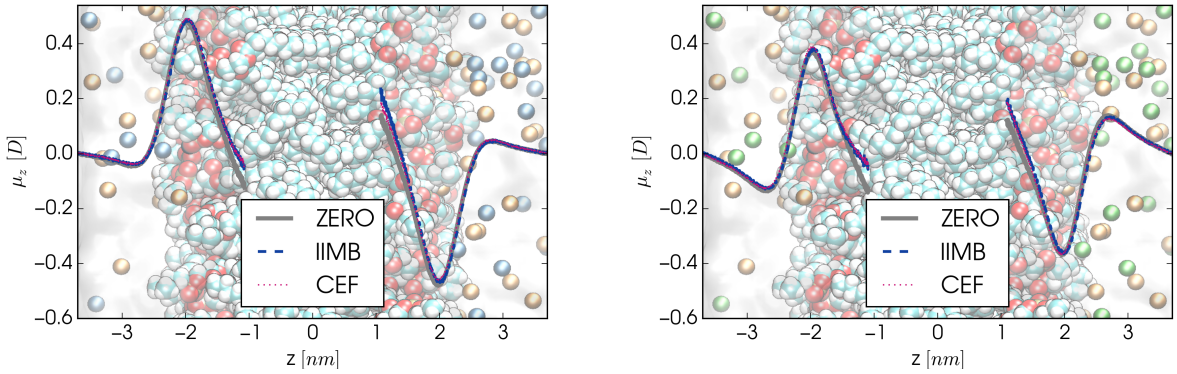


Figure 7: Profiles of the projection of water dipoles onto the membrane normal ($z$-axis). The only notable difference from the ZERO reference simulation lies solely in the carbonyl region, where the dipoles tend to orient in the direction of the induced electric field. The curves are cut at the point where the water density practically vanishes and the estimated error reaches 0.02 D.

directions on each of the two sides of the membrane. This cancels out their respective contributions to the electric field within the bilayer.[51]

The water ordering was analyzed by taking orientations of the water molecule dipoles and projecting them to the normal of the membrane, i.e., the $z$-axis. Note that with a non-zero transmembrane voltage, these dipoles do not balance out anymore and the membrane is under the influence of an additional induced electric field. The largest response to the transmembrane voltage is located at the interface between the polar (lipid headgroups) and non-polar (alkyl chains) layers of the membrane. In this region, the water dipoles accommodate to the induced electric field within the membrane with their altered orientation to the same extent in both types of simulations, CEF and IIMB (Fig. 7). This effect is, however, very weak for physiological transmembrane voltages. The mean orientation changes at most by one degree in the carbonyl region of the membrane, where the electrostatic screening is diminished by the vanishing water density and by the decreasing polarity of the membrane. Note also that the water dipoles in the FxI simulation have a matching profile with the ZERO reference simulation (not shown).

For the lipids, the voltage-related changes in their ordering are even smaller than for water. For high voltages close to the electroporation threshold a small decrease in the order parameter of lipids is observed with its maximum of 0.05 in the sn-1 chain of DOPC.[52] This corroborates our findings of a small but systematic decrease in the order parameter in both types of simulations, CEF and IIMB, which slightly disorders the POPC lipid bilayer (not shown). In addition, we observe only negligible changes up to one degree in the mean value of the P-N angle between the connector of the phosphate and choline groups and the membrane normal (Table 2). Note that studies done at a higher electric field close to the electroporation threshold showed a minor effect on the reorientation of the lipid headgroups.[22,53] At the threshold field for membrane poration, the external field changes the mean headgroup dipole angle by less than about 4° in the field direction.

From our simulations, we report that the mean value of the P-N angle is larger by approximately 4° for KCl than for NaCl background electrolyte, no matter if the external field is on or off. The headgroups are thus slightly more aligned with the normal of the membrane in the NaCl solution than in the KCl solution, pointing more toward the bulk water. This difference may be overestimated due to the neglect of polarizability in our simulations, which likely leads to a somewhat larger binding of $Na^+$ into phospholipidic membranes. As a result, the increased density of $Na^+$ in the headgroup region slightly lowers the water density at the interface and the area per molecule (not shown). It is known from the literature that sodium cations have a slightly higher affinity to PC lipids than potassium cations.[54,55] However, many studies suggest that sodium cations do not affect the structure of the membrane significantly.[56–58] More discussion on the interactions between cations and phospholipidic membranes can be found in previous articles on this topic.[42,55–63] In this work, we focus on the effects induced by voltage modulations, which are introduced by two different methods, i.e., constant electric field and ion imbalance. For the purpose of comparing the two methods, we can use the likely overestimated binding of $Na^+$ into POPC lipid membranes to our advantage, giving us an upper bound to the possible differences

Table 2: P-N angle values for KCl and NaCl simulations.

KCl

| Leaflet at | ZERO | CEF | IIMB | FxI |
|---|---|---|---|---|
| Zero potential | 67°± 3° | | | 67°± 3° |
| Positive potential | | 68°± 3° | 68°± 3° | 68°± 3° |
| Negative potential | | 67°± 3° | 67°± 3° | 68°± 3° |

NaCl

| | | | | |
|---|---|---|---|---|
| Zero potential | 63°± 3° | | | 64°± 4° |
| Positive potential | | 64°± 3° | 64°± 4° | 63°± 3° |
| Negative potential | | 63°± 3° | 63°± 4° | 63°± 3° |

between the two methods. More details including also the dynamical properties of the membrane are given in the SI.

# 4 Conclusion

To date, there exist two methods for modeling the transmembrane potential in molecular simulations. The method of the constant electric field represents the influence of a voltage source far in the aqueous bulk by an additional force acting on every charged particle.[14,16,17] This voltage source is an effective simplified model of the biological apparatus, i.e., ion pumps and channels, responsible for the existence of the transmembrane voltage in biological membranes. In the ion imbalance method the voltage is introduced by maintaining a metastable condition of unequal distribution of ions on the two sides of a membrane.[19,20] This is meant to mimic more closely the steady state situation at biological membranes maintained by the biological apparatus, where a small charge difference is responsible for a non-zero transmembrane voltage.

In this work, we have compared these two methods in biologically relevant model membrane systems. We achieved a considerable speed-up (about a factor of three) of the underlying molecular dynamics simulations by implementing the virtual interaction sites method for the Slipids force field. Based on these simulations, we showed that the two methods, i.e.,

constant electric field and ion imbalance, yield indistinguishable results within the statistical error. We compared important properties related to membrane electrostatics, such as the transmembrane potential, field intensity, and charge density. We have also introduced a more detailed quantity, the voltage-normalized differential charge density, which proved to be useful for the observation of charge redistributions. The profiles of these quantities along the membrane normal were shown to be matching for the two methods within the achievable accuracy. The two methods for modeling transmembrane voltage were also combined such as to cancel each other in a way that makes the potential drop vanish. This setup has given the same results as those obtained from a simulation with no transmembrane voltage. We thus conclude that the two methodologies are equivalent, at least for electrolytes formed by the same monovalent ions on both sides of the membrane, and can both be used to model the membrane potentials pertinent to electrophysiological or fluorescence experiments at model bilayers as well as living cells. Presented results thus directly connect together the practically independent developments within the two major approaches to transmembrane potential modeling – the constant electric field method[14,16,17] and the ion imbalance method.[19,23]

## Acknowledgement

We thank Hector Martinez-Seara and Josef Lazar for valuable comments. Support from the Czech Science Foundation (grant P208/12/G016), the Academy of Finland (FiDiPro award), and the Academy of Sciences (Praemium Academie award) is gratefully acknowledged. Computational resources were provided by the CESNET LM2015042 and the CERIT Scientific Cloud LM2015085 projects under the program "Projects of Large Research, Development, and Innovations Infrastructures". Simulations were performed using HPC resources from Jüllich Supercomputing Centre (Project hcz03) and on GENCI-TGCC (PRACE Project 2014112643).

## Supporting Information Available

The basic settings and input files for simulations and the figures validating virtual interaction sites and all-atom simulations are contained in the supporting information.

This material is available free of charge via the Internet at `http://pubs.acs.org/`.

## References


(1) Alberts, B.; Johnson, A.; Lewis, J.; Raff, M.; Roberts, K.; And Walter, P. *Molecular Biology of the Cell*; Garland Press: New York, 2008.

(2) Sten-Knudsen, O. *Biological Membranes: Theory of Transport, Potentials and Electric Impulses*; Cambridge University Press, 2002.

(3) Neher, E.; Sakmann, B. *Nature* **1976**, *260*, 799–802.

(4) Grinvald, A.; Salzberg, B. M.; Lev-Ram, V.; Hildesheim, R. *Biophys. J.* **1987**, *51*, 643–51.

(5) Han, Z.; Jin, L.; Chen, F.; Loturco, J. J.; Cohen, L. B.; Bondar, A.; Lazar, J.; Pieribone, V. A. *PLoS One* **2014**, *9*, e113873.

(6) Akemann, W.; Mutoh, H.; Perron, A.; Rossier, J.; Knöpfel, T. *Nat. Methods* **2010**, *7*, 643–9.

(7) Perron, A.; Mutoh, H.; Akemann, W.; Gautam, S. G.; Dimitrov, D.; Iwamoto, Y.; Knöpfel, T. *Front. Mol. Neurosci.* **2009**, *2*, 5.

(8) Mutoh, H.; Perron, A.; Dimitrov, D.; Iwamoto, Y.; Akemann, W.; Chudakov, D. M.; Knöpfel, T. *PLoS One* **2009**, *4*, e4555.

(9) Barnett, L.; Platisa, J.; Popovic, M.; Pieribone, V. A.; Hughes, T. *PLoS One* **2012**, *7*, e43454.

(10) Lei Jin, Zhou Han, Jelena Platisa, Julian R. A. Wooltorton, L. B. C.; Pieribone, V. A. *NIH* **2012**, *75*, 779–785.

(11) Akemann, W.; Lundby, A.; Mutoh, H.; Knöpfel, T. *Biophys. J.* **2009**, *96*, 3959–76.

(12) Fisher, J. A. N.; Barchi, J. R.; Welle, C. G.; Kim, G.-H.; Kosterin, P.; Obaid, A. L.; Yodh, A. G.; Contreras, D.; Salzberg, B. M. *J. Neurophysiol.* **2008**, *99*, 1545–53.

(13) Obaid, A. L.; Loew, L. M.; Wuskell, J. P.; Salzberg, B. M. *J. Neurosci. Methods* **2004**, *134*, 179–90.

(14) Roux, B. *Biophys. J.* **1997**, *73*, 2980–2989.

(15) Tieleman, D. P.; Berendsen, H. J. C.; Sansom, M. S. P. *Biophys. J.* **2001**, *80*, 331–346.

(16) Roux, B. *Biophys. J.* **2008**, *95*, 4205–4216.

(17) Gumbart, J.; Khalili-Araghi, F.; Sotomayor, M.; Roux, B. *Biochim. Biophys. Acta, Biomembr.* **2012**, *1818*, 294–302.

(18) Sin, J.-S.; Im, S.-J.; Kim, K.-I. *Electrochim. Acta* **2015**, *153*, 531–539.

(19) Sachs, J. N.; Nanda, H.; Petrache, H. I.; Woolf, T. B. *Biophys. J.* **2004**, *86*, 3772–3782.

(20) Delemotte, L.; Dehez, F.; Treptow, W.; Tarek, M. *J. Phys. Chem. B* **2008**, *112*, 5547–5550.

(21) Vargas, E.; Yarov-Yarovoy, V.; Khalili-Araghi, F.; Catterall, W. A.; Klein, M. L.; Tarek, M.; Lindahl, E.; Schulten, K.; Perozo, E.; Bezanilla, F.; Roux, B. *J. Gen. Physiol.* **2012**, *140*, 587–94.

(22) Böckmann, R. A.; de Groot, B. L.; Kakorin, S.; Neumann, E.; Grubmüller, H. *Biophys. J.* **2008**, *95*, 1837–1850.

(23) Kutzner, C.; Grubmüller, H.; de Groot, B. L.; Zachariae, U. *Biophys. J.* **2011**, *101*, 809–817.

(24) Casciola, M.; Bonhenry, D.; Liberti, M.; Apollonio, F.; Tarek, M. *Bioelectrochemistry* **2014**, *100*, 11–17.

(25) Delemotte, L.; Tarek, M. *J. Membrane Biol.* **2012**, *245*, 531–543.

(26) Andelman, D. *Handb. Biol. Phys.* **1995**, *1*, 603–642.

(27) Gurtovenko, A. A.; Vattulainen, I. *J. Phys. Chem. B* **2009**, *113*, 7194–7198.

(28) Vernier, P. T.; Ziegler, M. J.; Sun, Y.; Gundersen, M. A.; Tieleman, D. P. *Phys. Biol.* **2006**, *3*, 233–247.

(29) Jämbeck, J. P. M.; Lyubartsev, A. P. *J. Chem. Theory Comput.* **2012**, *8*, 2938–2948.

(30) Jämbeck, J. P. M.; Lyubartsev, A. P. *J. Phys. Chem. B* **2012**, *116*, 3164–3179.

(31) Mahoney, M. W.; Jorgensen, W. L. *J. Chem. Phys.* **2000**, *112*, 8910–8922.

(32) Smith, D. E.; Dang, L. X. *J. Chem. Phys.* **1994**, *100*, 3757.

(33) Chang, T.-M.; Dang, L. X. *J. Phys. Chem. B* **1999**, *103*, 4714–4720.

(34) Hess, B.; Kutzner, C.; van der Spoel, D.; Lindahl, E. *J. Chem. Theory Comput.* **2008**, *4*, 435–447.

(35) Darden, T.; York, D.; Pedersen, L. *J. Chem. Phys.* **1993**, *98*, 10089–10092.

(36) Páll, S.; Hess, B. *Comput. Phys. Commun.* **2013**, *184*, 2641–2650.

(37) Bussi, G.; Donadio, D.; Parrinello, M. *J. Chem. Phys.* **2007**, *126*, 014101.

(38) Parrinello, M.; Rahman, A. *J. Phys. D. Appl. Phys.* **1981**, *52*, 7182–7190.

(39) Hess, B.; Bekker, H.; Berendsen, H. J. C.; Fraaije, J. G. E. M. *J. Comput. Chem.* **1997**, *18*, 1463–1472.

(40) Miyamoto, S.; Kollman, P. A. *J. Comput. Chem.* **1992**, *13*, 952–962.

(41) Arkhipov, A.; Yin, Y.; Schulten, K. *Biophys. J.* **2008**, *95*, 2806–2821.

(42) Böckmann, R. A.; Hac, A.; Heimburg, T.; Grubmüller, H. *Biophys. J.* **2003**, *85*, 1647–1655.

(43) Feenstra, K. A.; Hess, B.; Berendsen, H. J. C. *J. Comput. Chem.* **1999**, *20*, 786–798.

(44) Bjelkmar, P.; Larsson, P.; Cuendet, M. A.; Hess, B.; Lindahl, E. *J. Chem. Theory Comput.* **2010**, *6*, 459–466.

(45) Aponte-Santamaría, C.; Briones, R.; Schenk, A. D.; Walz, T.; Groot, B. L. d. *Proc. Natl. Acad. Sci. U.S.A* **2012**, *109*, 9887–9892.

(46) Loubet, B.; Kopec, W.; Khandelia, H. *J. Chem. Theory Comput.* **2014**, *10*, 5690–5695.

(47) Paloncýová, M.; Fabre, G.; DeVane, R. H.; Trouillas, P.; Berka, K.; Otyepka, M. *J. Chem. Theory Comput.* **2014**, *10*, 4143–4151.

(48) Goldman, D. E. *J. Gen. Physiol.* **1943**, *27*, 37–60.

(49) Troiano, G. C.; Tung, L.; Sharma, V.; Stebe, K. J. *Biophysical J.* **1998**, *75*, 880–8.

(50) Wang, L. *Annu. Rev. Biochem.* **2012**, *81*, 615–35.

(51) Tieleman, D. P. *BMC Biochem.* **2004**, *5*, 10.

(52) Gurtovenko, A. A.; Lyulina, A. S. *J. Phys. Chem. B* **2014**, *118*, 9909–9918.

(53) Ziegler, M. J.; Vernier, P. T. *J. Phys. Chem. B* **2008**, *112*, 13588–13596.

(54) Gurtovenko, A. A.; Vattulainen, I. *J. Phys. Chem. B* **2008**, *112*, 1953–1962.

(55) Jurkiewicz, P.; Cwiklik, L.; Vojtíšková, A.; Jungwirth, P.; Hof, M. *Biochim. Biophys. Acta Biomembranes* **2012**, *1818*, 609–616.

(56) Botan, A.; Fernando, F.; Fuchs, P. F. J.; Javanainen, M.; Kanduc, M.; Kulig, W.; Lamberg, A.; Loison, C.; Lyubartsev, A. P.; Miettinen, M. S.; Monticelli, L.; Määttä, J.; Ollila, S. O.; Retegan, M.; Róg, T.; Santuz, H.; Tynkkynen, J. P. *J. Phys. Chem. B* **2015**,

(57) Gurtovenko, A. a. *J. Chem. Phys.* **2005**, *122*, 244902.

(58) Venable, R. M.; Luo, Y.; Gawrisch, K.; Roux, B.; Pastor, R. W. *J. Phys. Chem. B* **2013**, *117*, 10183–10192.

(59) Berkowitz, M. L.; Vácha, R. *Acc. Chem. Res.* **2012**, *45*, 74–82.

(60) Lee, S.-J.; Song, Y.; Baker, N. A. *Biophys. J.* **2008**, *94*, 3565–76.

(61) Pandit, S. A.; Bostick, D.; Berkowitz, M. L. *Biophys. J.* **2003**, *84*, 3743–50.

(62) Vácha, R.; Siu, S. W. I.; Petrov, M.; Böckmann, R. a.; Barucha-Kraszewska, J. J.; Jurkiewicz, P.; Hof, M.; Berkowitz, M. L.; Jungwirth, P. *J. Phys. Chem. A* **2009**, *113*, 7235–7243.

(63) Vácha, R.; Jurkiewicz, P.; Petrov, M.; Berkowitz, M. L.; Böckmann, R. a.; Barucha-Kraszewska, J.; Hof, M.; Jungwirth, P. *J. Phys. Chem. B* **2010**, *114*, 9504–9509.

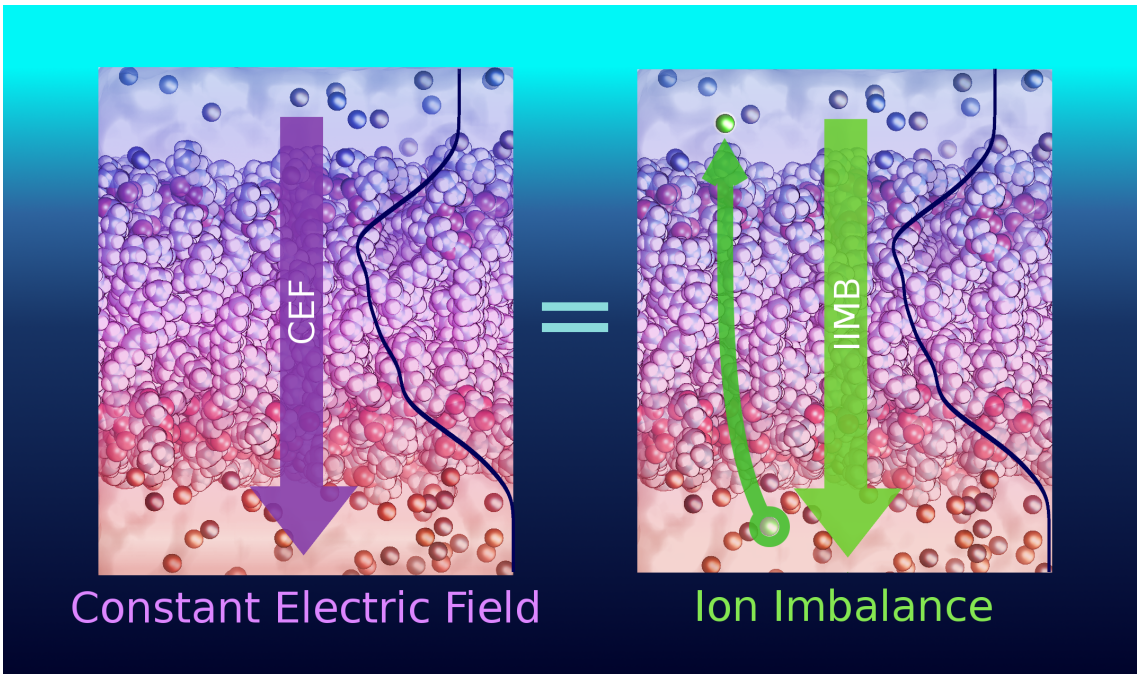


For Table of Contents Only